Progress In Electromagnetics Research, Vol. 123, 371–384, 2012

NEW DUAL-BAND BANDPASS FILTER WITH WIDE UPPER REJECTION BAND

J.-T. Kuo[1,*] and S.-W. Lai[2]

[1]Department of Electronic Engineering, Chang Gung University, Taoyuan, Taiwan

[2]Mediatek Corp., Hsinchu, Taiwan

Abstract—A new circuit structure is proposed for design of dual-band bandpass filters with a wide upper stopband. The unit cell of the circuit consists of two two-port networks in shunt connection; one is a coupled-line section of $\lambda/4$ long followed by a transmission line segment of identical length, and the other has the same elements but cascaded in reverse order, where $\lambda/4$ is the wavelength at arithmetic mean frequency of the two passbands. Higher-order circuits can be obtained by directly cascading two or more such cells and show improved frequency selectivity. In addition to on both sides of the passbands, transmission zeros are also created in the rejection bands. Analysis of the unit cell circuit is formulated by the transmission line theory, and design curves for one- and two-cell circuits are provided. In realization, interdigital capacitors are incorporated with the $\lambda/4$ coupled sections for compensating the effect of unequal modal phase velocities on the filter performance in the rejection band. Two circuits are fabricated and measured to validate the analysis.

1. INTRODUCTION

Dual-band bandpass filter design has been a hot research topic recently [1–15]. In contrast to traditional single-band filters, the design has to take care of the passband functions and bandwidths of the two passbands. The stepped-impedance resonator is suitable for such design since the ratio of its fundamental and the second resonant frequencies can be easily tuned by its geometric parameters [1–3]. In [2], the circuit bandwidths at the two designated bands can be well controlled using a so-called bandwidth design graph in readiness. If

Received 23 November 2011, Accepted 22 December 2011, Scheduled 31 December 2011

* Corresponding author: Jen-Tsai Kuo (jtkuo123@mail.cgu.edu.tw).

some inherent properties of the coupling structure are incorporated into the design, transmission zeros can be created at the desired positions, then a wide upper stopband can be achieved at the same time [3]. Straight resonators loaded with shunt stubs are also good candidates for the dual-band purpose [4, 5], since the ratio of the two resonant frequencies can be easily changed by altering the length and the characteristic impedance of the stub.

Dual-band filters can also be designed with a compact size [6, 7]. Dual-mode resonator is also attractive for filter design with a dual-passband response due to its compact area and low cost. A single ring resonator can also be used to build a dual-mode dual-band bandpass filter [8]. The ring peripheral is deformed into several microwave C-sections; each of them plays the role of a $\lambda/4$- or $\lambda/6$-section (at the first frequency) of a traditional ring. In [9], the circuit is a multilayer structure consisting of dual-mode resonators in a reflector cavity. In [10], a new dual-mode dual-band filter is devised by a single stepped-impedance resonator with two quasi-elliptic function passbands.

There have been many other innovative dual-band filters published recently [11–15]. In [11], the dual-band bandpass filter is designed by a dual feeding structure and embedded uniform impedance resonator. The two passbands can be designed individually and several transmission zeros can be created to improve the frequency selectivity and circuit performance in stopband. In [12], a systematic synthesis procedure is described for a fully controllable second passband. On the basis of this idea, flexible passband and bandwidth selections can be achieved by treating a stepped-impedance coupled-line as a dual-band inverter [13]. In [14], a dual-wideband filter is implemented by stepped-impedance resonators incorporating with the frequency mapping approach. In [15], beginning with a low-pass prototype, a dual-band bandpass filter is obtained by implementing successive frequency transformations and circuit conversions.

In this paper, based on the development in [16], a new filter structure is devised for creating dual-band bandpass responses. The two passbands are separated by a transmission zero at the center frequency. The unit cell is a one-stage circuit consisting of two coupled-line sections and two transmission line segments of $\lambda/4$ long, where $\lambda/4$ is the center of the two passband frequencies. The circuit order can be easily increased by simply cascading the unit cells. It is found that the unequal even and odd mode phase velocities will degrade the filter performance in rejection band, especially when a high-ε_r substrate is used. Interdigital capacitors are employed along with all the $\lambda/4$ coupled sections to compensation this effect and to recover the rejection

levels obtained by simulation with the ideal transmission line model.

This paper is organized as follows. Section 2 formulates the analysis of the one-stage circuit. Several design graphs for one- and two-stage filters are provided for facilitating the circuit synthesis. Section 3 demonstrates the measured data of two experimental circuits and compares with the simulation, and Section 4 draws the conclusion.

2. CIRCUIT STRUCTURE AND ANALYSIS

Figure 1(a) shows the proposed dual-band filter structure. It is a cascade of two unit cells, and each cell, as shown in Figure 1(b), is a dual-band bandpass filter of the second order. Before the circuit in Figure 1(a) is designed, the transmission characteristics of the unit cell in Figure 1(b) are analyzed as follows. From the input to the output, the upper signal path is a coupled-line followed by a transmission line section with characteristic impedance Z_T, and the lower path has the same components placed in a reverse order. The electrical length of each section is $\theta = 90^\circ$ at the center frequency f_0. The $ABCD$ matrices for the coupled-line and the transmission line sections are [17]

$$\begin{bmatrix} A & B \\ C & D \end{bmatrix}_C = \frac{\sin\theta}{T} \begin{bmatrix} qU & j\frac{P}{2} \\ j2 & qU \end{bmatrix} \tag{1a}$$

$$\begin{bmatrix} A & B \\ C & D \end{bmatrix}_L = \sin\theta \begin{bmatrix} q & jz_1 \\ jy_1 & q \end{bmatrix} \tag{1b}$$

$$P = T^2 + q^2\left(T^2 - U^2\right) \tag{1c}$$

$$U = \frac{Z_{0e} + Z_{0o}}{Z_o} \equiv z_e + z_o \tag{1d}$$

$$T = \frac{Z_{0e} - Z_{0o}}{Z_o} \equiv z_e - z_o \tag{1e}$$

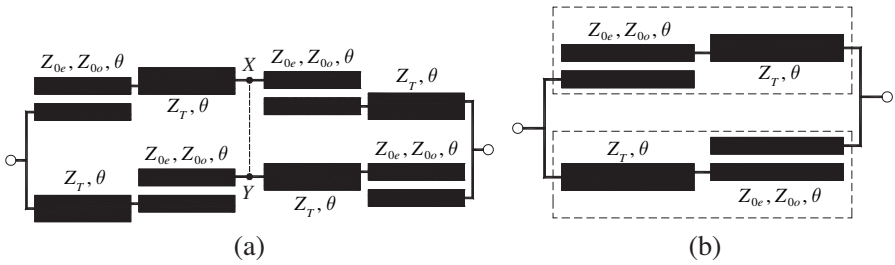

Figure 1. (a) Proposed dual-band filter with a cascade of two unit cells. (b) Unit cell.

where Z_{0e} and Z_{0o} are the even and odd mode characteristic impedances of the coupled-line, respectively, $z_e = Z_{0e}/Z_0$, $z_o = Z_{0o}/Z_0$, $z_1 = Z_T/Z_0$, $y_1 = 1/z_1$, and $q = \cot\theta$. The subscripts C and L represent the coupled-line and the transmission line sections, respectively. The $ABCD$ matrix for the upper signal path can be obtained by multiplying the matrices in (1a) and (1b). It can be validated that the $ABCD$ matrix of the lower path is that of the upper one by switching A and D. Then, the S-parameters of the entire network in Figure 1(b) can be derived by adding the two admittance matrices converted from these two $ABCD$ matrices

$$S_{11} = S_{22} = \frac{B^2 - (A^2 - 1)}{(A + B + 1)(A + B - 1)} \tag{2a}$$

$$S_{21} = S_{12} = \frac{2B}{(A + B + 1)(A + B - 1)} \tag{2b}$$

$$A = \frac{\sin^2\theta}{2T}\left[2q^2U - \frac{y_1}{2}P - 2z_1\right] \tag{2c}$$

$$B = j\frac{\sin^2\theta}{2T}q\left[Uz_1 + \frac{1}{2}P\right] \tag{2d}$$

where the A and B are the entries of the transmission matrix of the circuit in Figure 1(b). It can be expected that the filter response will be symmetric about $2f_0$ ($\theta = \pi$), which is an inherent distributed nature of the transmission line network. Also, the $|S_{11}|$ and $|S_{21}|$ responses will also be symmetric about f_0, since the magnitudes of all θ-related functions in (2) are symmetric about $\theta = \pi/2$. It leads to that the bandwidths of the two passbands will be identical. Enforcing $S_{21} = 0$ yields the transmission zeros of the circuit:

$$q = 0,\ \pm\sqrt{\frac{2Uz_1 + T^2}{U^2 - T^2}},\ \pm\infty \tag{3}$$

The solutions $q = 0$ and $\pm\infty$ correspond to $\theta = n\pi/2$ (or $f = nf_0$), $n = 0, 1, 2, \ldots$. Note that the solutions at f_0 and $3f_0$ are inherent transmission zeros of the coupled-line sections [18]. The transmission poles of the unit cell, on the other hand, can be calculated from (2a) by enforcing $B^2 = A^2 - 1$. It results in a sixth-order equation of q:

$$\alpha^2q^6 + \left(\beta^2 + 2\alpha\chi - 16T^2\right)q^4 + \left(\chi^2 - 2\beta\delta - 32T^2\right)q^2 + \delta^2 - 16T^2 = 0 \tag{4a}$$

where

$$\alpha = T^2 - U^2 \tag{4b}$$

$$\beta = 4U - \alpha y_1 \tag{4c}$$

$$\chi = 2Uz_1 + T^2 \tag{4d}$$

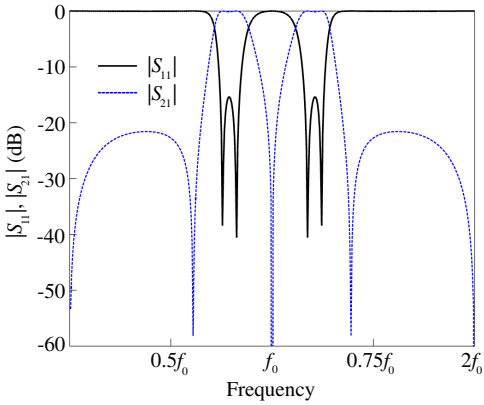

Figure 2. $|S_{11}|$ and $|S_{21}|$ responses of the unit cell in Figure 1(b). $z_e = 2.18$, $z_o = 1.68$, $z_1 = 0.9$.

$$\delta = y_1 T^2 + 4z_1 \tag{4e}$$

Equation (4a) consists of even order terms only, thus it can be solved by using the cubic formula in [19]. Our numerical experiments show that q^2 has one negative and two positive roots. The negative root should be ignored since q is real, and the two positive roots imply that the unit cell is a second-order circuit. It is reasonable since the unit cell in Figure 1(b) possesses at most two resonators only.

Figure 2 plots calculated $|S_{11}|$ and $|S_{21}|$ responses versus normalized frequency with $z_e = 2.18$, $z_o = 1.68$, and $z_1 = 0.9$. The inband $|S_{11}|$ is better than -15 dB and $|S_{21}|$ levels better than -20 dB in the stopbands. These levels depend on the values of z_e, z_o, and z_1. Design graphs will be demonstrated later for this circuit.

The circuit shown in Figure 1(a) is a cascade of two identical unit cells in Figure 1(b). Along the upper signal path, node X is the midway from the input to the output. Thus, the voltage at this point is the arithmetic average of those applied to the input and output ports. Based on the same idea, the voltage at point Y is also the average of the voltages at the input and output ports, and it is the same as the voltage at X. Therefore, when two unit cells are cascaded, the interconnection between X and Y can be removed without changing any circuit property at all frequencies. Apparently, higher order circuits can be analyzed in a similar way. The attenuation levels in the stopband will be improved. This point has been validated by our simulation. None of even higher-order circuits will be shown herein since a two-stage circuit is capable of providing insertion losses of $40 \sim 50$ dB in the stopbands.

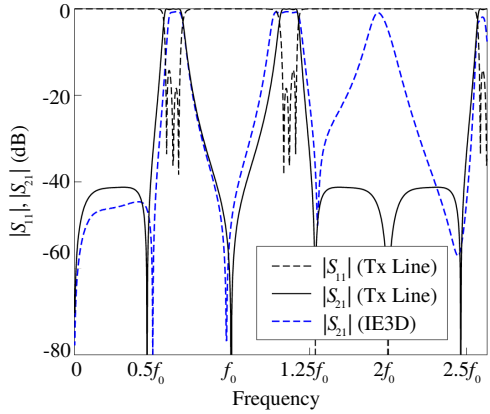

Figure 3. $|S_{11}|$ and $|S_{21}|$ responses for the two-stage circuit. $z_e = 0.78$, $z_o = 0.6$, $z_1 = 0.8$. The IE3D [20] results are obtained by using $Z_{0e} = 39\,\Omega$, $Z_{0o} = 30\,\Omega$, $Z_T = 40\,\Omega$ on a substrate with $\varepsilon_r = 10.2$ and thickness $= 0.635\,\text{mm}$. $f_{c1} = 2.4\,\text{GHz}$, $f_{c2} = 5.2\,\text{GHz}$, $f_0 = 3.8\,\text{GHz}$.

Figure 3 plots the calculated $|S_{11}|$ and $|S_{21}|$ responses for the two-cell filter with $z_e = 0.78$, $z_o = 0.6$, $z_1 = 0.8$. In general, the rejection levels in the stopband are much better than those of the one-stage filter. Each passband shows three transmission poles. The transmission zeros of this two-stage filter are the same as the one-stage circuit if z_e, z_o and z_1 are not changed. It can be explained as follows. The $ABCD$ matrix of the entire two-stage circuit is the square of the $ABCD$ matrix of a unit cell. Thus, the B-element of the entire two-stage circuit will be $AB+BD = 2AB = 0$ where A and B are in (2c) and (2d), respectively. Note that in (2b) and (2d) $B = 0$ is used to find the transmission zeros.

3. DESIGN GRAPHS

Although the design variables include three variables (z_e, z_o and z_1) only, the proposed circuits possess satisfactory filter characteristics in both passband and stopband, as well as a wide tuning range of the ratio of the two passband frequencies, if these three variables can be properly chosen. Referring to the responses in Figure 2, important filter characteristics in this design include the frequency ratio of the two passbands (R_{freq}), circuit bandwidth (Δ), maximal $|S_{21}|$ level (R_{stop}, in dB) in the stopbands and the maximal inband $|S_{11}|$ level (R_{pass}, in dB) in the passbands. The fractional bandwidth Δ of the proposed circuit is defined in a way similar to, but not the same as the traditional

Chebyshev response. As shown in Figure 4, the R_{pass} level in the first passband determines $f_{1\pm}$, then

$$\Delta = \frac{f_{1+} - f_{1-}}{f_{c1}} \times 100\% \tag{5a}$$

$$f_{c1} = \frac{f_{1+} + f_{1-}}{2} \tag{5b}$$

where the center frequency of the first passband f_{c1} is chosen as arithmetic average of f_{1+} and f_{1-}. The second passband frequency f_{c2} is then $2f_0 - f_{c1}$. It is known that the two passbands of the filter have the same absolute bandwidths, so the fractional bandwidth in (5a) applies to the first band only.

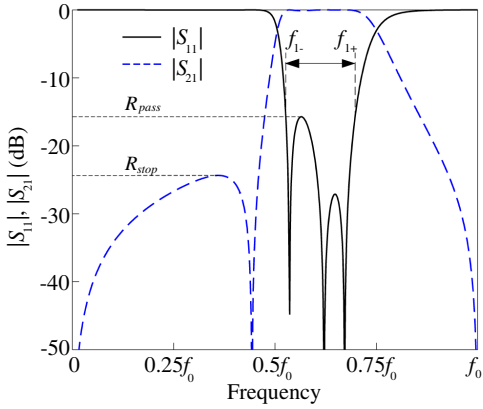

Figure 4. Definitions of R_{stop}, R_{pass} and relative bandwidth Δ.

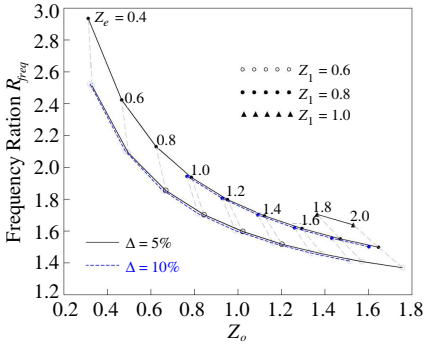

Figure 5. Design graph for one-stage circuit in Figure 1(b).

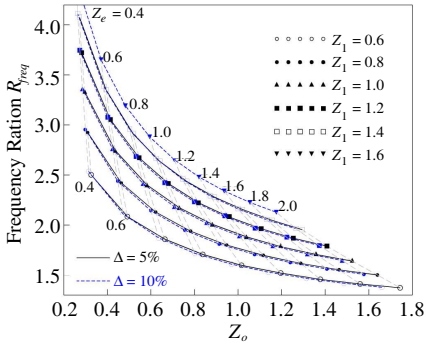

Figure 6. Design graph for two-stage circuit.

Figures 5 and 6 plot design graphs for the one-stage and two-stage circuits, respectively. These data are obtained, based on the formulation in (1)–(3), by first setting z_1 and z_e, then searching the z_o value fulfilling $\Delta = 5\%$ or 10%. The corresponding levels of R_{pass} and R_{stop} are listed in Tables 1 through 4. The data have also been validated by the Agilent ADS® with the ideal transmission line models.

Figure 5 shows the R_{freq} solution versus z_o for $z_1 = 0.6$, 0.8 and

Table 1. R_{stop} (dB) and R_{pass} (dB) of one-stage circuit with $\Delta = 5\%$.

$\Delta = 5\%$		z_e									
		0.4		0.8		1.2		1.6		2.0	
		R_{stop}	R_{pass}	R_{stop}	R_{pass}	R_{stop}	R_{pass}	R_{stop}	R_{pass}	R_{stop}	R_{pass}
z_1	0.6	−22.4	−25.2	−24.5	−23.9	−26.7	−22.5	−28.7	−20.8	−30.4	−19.0
	0.8	−19.5	−28.6	−20.6	−29.9	−22.0	−28.7	−23.4	−27.4	−24.8	−25.7
	1.0	−17.5	−31.9	−17.7	−33.8	−18.6	−33.6	−19.5	−33.0	−20.5	−32.0

Table 2. R_{stop} (dB) and R_{pass} (dB) of one-stage circuit with $\Delta = 10\%$.

$\Delta = 10\%$		z_e									
		0.4		0.8		1.2		1.6		2.0	
		R_{stop}	R_{pass}	R_{stop}	R_{pass}	R_{stop}	R_{pass}	R_{stop}	R_{pass}	R_{stop}	R_{pass}
z_1	0.6	−21.1	−14.1	−23.1	−13.7	−25.0	−12.2	−26.7	−10.8	−28.2	−9.7
	0.8	−18.7	−17.5	−19.7	−18.1	−21.1	−17.7	−22.4	−16.7	−23.6	−15.7
	1.0	−16.9	−20.4	−17.2	−22.2	−18.0	−21.9	−18.9	−21.7	−19.8	−21.1

Table 3. R_{stop} (dB) and R_{pass} (dB)of two-stage circuit with $\Delta = 5\%$.

$\Delta = 5\%$		z_e									
		0.4		0.8		1.2		1.6		2.0	
		R_{stop}	R_{pass}	R_{stop}	R_{pass}	R_{stop}	R_{pass}	R_{stop}	R_{pass}	R_{stop}	R_{pass}
z_1	0.6	−49.6	−25.2	−53.8	−28.8	−56.3	−28.2	−58.7	−27.7	−60.8	−21.6
	0.8	−44.5	−30.8	−46.1	−35.9	−47.5	−35.5	−49.3	−35.1	−51.3	−35.8
	1.0	−40.7	−32.2	−40.3	−38.6	−41.0	−40.2	−42.2	−40.1	−43.7	−41.6
	1.2	−37.5	−33.3	−36.0	−39.2	−35.9	−42.4	−36.6	−42.7	−37.6	−45.6
	1.4	−35.3	−38.1	−32.9	−53.4	−32.0	−44.3	−32.1	−44.1	−32.7	−46.3

Table 4. R_{stop} (dB) and R_{pass} (dB) of two-stage circuit with $\Delta = 10\%$.

Δ = 10%		z_e									
		0.4		0.8		1.2		1.6		2.0	
		R_{stop}	R_{pass}	R_{stop}	R_{pass}	R_{stop}	R_{pass}	R_{stop}	R_{pass}	R_{stop}	R_{pass}
z_1	0.6	−46.6	−15.1	−50.1	−15.5	−52.0	−14.6	−53.9	−12.5	−55.3	−10.4
	0.8	−42.4	−19.1	−43.7	−20.6	−45.0	−20.9	−46.5	−20.5	−48.2	−18.3
	1.0	−39.8	−20.9	−38.7	−23.6	−39.4	−25.0	−40.6	−25.2	−41.8	−25.7
	1.2	−36.1	−22.3	−34.9	−26.0	−34.9	−28.0	−35.4	−28.5	−36.4	−29.6
	1.4	−34.0	−23.8	−31.7	−27.0	−31.1	−29.3	−31.3	−30.8	−31.9	−32.0
	1.6	−32.7	−29.5	−29.6	−34.2	−28.5	−36.4	−28.2	−37.0	−28.3	−37.8

1. When $\Delta = 5\%$ and $z_1 = 0.6$, as z_e is varied from 0.4 to 2.0, the frequency ratio R_{freq} goes down from 2.51 to 1.37. When z_1 is increased to 0.8, the R_{freq} solution covers a range from 2.94 to 1.5. If $z_1 = 1$ is used, however, the R_{freq} results are between 1.64 and 1.70 for $1.8 \leq z_e \leq 2.0$. It is difficult to find solutions for structures with z_1 greater than unity. It should be paid attention that the R_{freq} data for $\Delta = 10\%$ are close to those for $\Delta = 5\%$. As shown Table 1, when z_1 is increased from 0.6 to 1, the inband R_{pass} level gets better and better, but the R_{stop} results becomes higher and higher. When z_e is changed from 0.4 to 2.0 step by step, the stopband rejection level improves gradually but the inband return loss degrades at the same time. In comparison with the results for $\Delta = 5\%$, the R_{stop} levels for $\Delta = 10\%$ in Table 2 are $0.5 \sim 2$ dB higher, but the R_{pass} may be increased up to more then 10 dB. Note that there are solutions ($z_1 = 0.8$ and $1.2 \leq z_e \leq 1.6$) to the one-stage circuit having $\Delta = 10\%$ with $R_{pass} \leq -16.4$ dB (inband ripple ≤ 0.1 dB) and $R_{stop} \leq -20$ dB.

Figure 6 plots the design curves for the two-stage circuit in Figure 1(a), and Tables 3 and 4 list the corresponding R_{stop} and R_{pass} levels. The numbers of R_{freq} and z_o solutions are more than those for the one-stage circuits as z_e is changed from 0.4 to 2.0. The z_1 value is given up to 1.6. The variation trends of R_{stop} and R_{pass} for changing z_1 and varying z_e values are similar to those for the one-stage circuit. The R_{stop} levels in Table 3 are $20 \sim 30$ dB better than those in Table 1 for the same z_1 and z_e, and the R_{pass} values also show some improvements. Note that the same z_1 and z_e values used in one- and two-stage circuits result in different R_{freq} ratios. For the circuits with $\Delta = 10\%$, most of the R_{pass} data in Table 4 show improvement from those in Table 2 of $1 \sim 4$ dB. The passband ripple can be greatly reduced by using $z_1 = 1.2 \sim 1.6$.

4. SIMULATION AND MEASUREMENT

The section demonstrates some measured data of two experimental circuits realized by the microstrip technology. The circuits are designed on a substrate with $\varepsilon_r = 10.2$ and thickness $= 0.635\,\text{mm}$, and the electromagnetic simulation herein is done by the software package IE3D [20].

One of the fundamental disadvantages of microstrip circuits with coupled-line sections that make the filter performance away from the ideal transmission line model is the unequal even and odd mode phase velocities. The issue becomes more serious when a substrate with high dielectric constant is used. Figure 3 also plots the $|S_{21}|$ response with microstrip realization. A spurious peak close to 0 dB with relatively large bandwidth at $1.8f_0$ can be observed. The simulated microstrip circuit has a substrate of $\varepsilon_r = 10.2$ and thickness $= 0.635\,\text{mm}$. The design parameters include $Z_{0e} = 39\,\Omega$, $Z_{0o} = 30\,\Omega$, $Z_T = 40\,\Omega$ at $f_0 = 3.8\,\text{GHz}$. This problem can be tackled by inserting shunt capacitors between the coupled lines [21]. Let the capacitance value of the capacitor be denoted by C_{comp}. The interdigital structure [22] is used to implement such capacitors. In this way, the physical length of the coupled-line section is determined by the effective dielectric constant of the even mode. Note also in Figure 3 that the microstrip

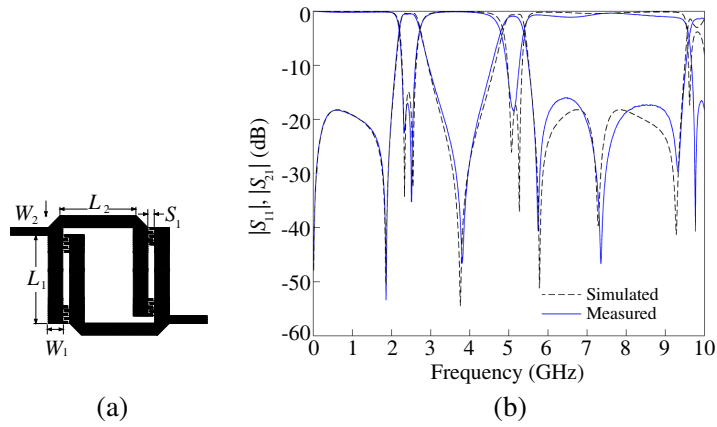

Figure 7. (a) Circuit layout and (b) simulated and measured $|S_{11}|$ and $|S_{21}|$ responses for the fabricated one-stage circuit designed at $f_{c1} = 2.4\,\text{GHz}$ and $f_{c2} = 5.2\,\text{GHz}$. $Z_{0e} = 39\,\Omega$, $Z_{0o} = 30\,\Omega$, $Z_T = 40\,\Omega$, $C_{comp} = 0.055\,\text{pF}$. $S_1 = 0.54\,\text{mm}$, $W_1 = 1.16\,\text{mm}$, $W_2 = 0.91\,\text{mm}$, $L_1 = 6.91\,\text{mm}$, $L_2 = 6.09\,\text{mm}$.

structure also alters the circuit bandwidths.

Figure 7(a) draws the layout for a one-stage circuit designed to have $f_{c1} = 2.4\,\text{GHz}$ and $f_{c2} = 5.2\,\text{GHz}$. Figure 7(b) shows that the simulated and measured results have good agreement. The circuit is designed to have $R_{stop} = -20\,\text{dB}$ by the Agilent ADS®, but the realization has $R_{stop} = -16.1\,\text{dB}$ at 6.5 GHz. The value of C_{comp} is 0.055 pF, evaluated at $2f_0 = 7.6\,\text{GHz}$. The line width and gap size of the interdigital capacitors are 0.15 mm. Five fingers are used and their lengths are 0.39 mm. One can observe that the four interdigital capacitors compensate the inequality of modal phase velocities quite well, so that the resultant transmission zero is close to $2f_0$ can be retained and the neighboring rejection can keep at a low level. The circuit occupies an area of $9.3 \times 9.6\,\text{mm}^2$. The measured insertion losses at f_{c1} and f_{c2} are $-0.55\,\text{dB}$ and $-1.04\,\text{dB}$, respectively.

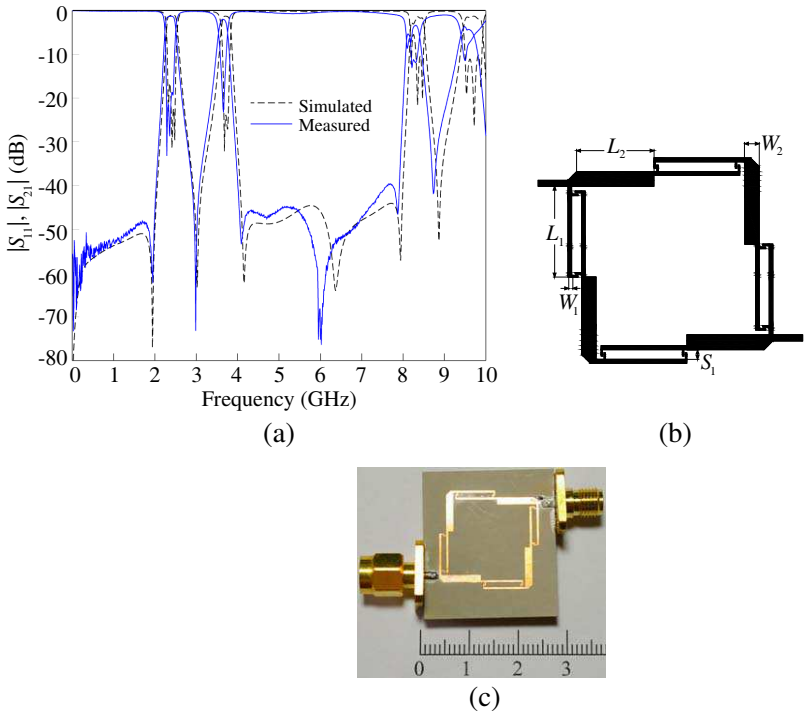

Figure 8. (a) Simulated and measured $|S_{11}|$ and $|S_{21}|$ responses, (b) circuit layout, and (c) circuit photograph for the fabricated two-stage circuit designed at $f_{c1} = 2.4\,\text{GHz}$ and $f_{c2} = 3.7\,\text{GHz}$. $Z_{0e} = 65\,\Omega$, $Z_{0o} = 56\,\Omega$, $Z_T = 30\,\Omega$, $C_{comp} = 0.0258\,\text{pF}$. $S_1 = 0.99\,\text{mm}$, $W_1 = 0.38\,\text{mm}$, $W_2 = 1.47\,\text{mm}$, $L_1 = 9.15\,\text{mm}$, $L_2 = 7.79\,\text{mm}$.

Figure 8(a) draws the layout for the realized two-stage dual-band filter with passbands at $f_{c1} = 2.4\,\text{GHz}$ and $f_{c2} = 3.7\,\text{GHz}$, and Figure 8(b) compares the measured responses with the simulated results. The R_{freq} ratio is lower than that in Figure 7 so that both the even and odd mode characteristic impedances should be increased, based on the data shown in Figure 6, i.e., the coupled-line has a smaller line width and gap size. The measured insertion losses at f_{c1} and f_{c2} are $-1.3\,\text{dB}$ and $-2.3\,\text{dB}$, respectively, and that the rejection levels in the stopband are better than 40 dB before 8 GHz. The inherent transmission zero at 6.1 GHz of the coupled-line stages designed at 3.05 GHz is recovered by $C_{comp} = 0.0258\,\text{pF}$. Each capacitor uses the same width and gap size as that in Figure 7. Two fingers are required for this case, and their lengths are 0.64 mm. Figure 8(c) is the photograph of the measured circuit. The circuit occupies an area of $20.7 \times 20.7\,\text{mm}^2$.

5. CONCLUSION

A new building block for constructing dual-band bandpass filters is proposed. The block consists of two subcircuits in shunt connection. The upper subcircuit is a cascade of a coupled-line and a transmission line section; both are of quarter-wavelength at the midpoint of the two designated passbands. The lower subcircuit possesses the same constitutes as the upper one, but they are cascaded in reverse order. It is shown that higher-order circuits can be obtained by directly cascading the one-stage circuits. The design graphs for one- and two-stage circuits are provided and discussed. It shows that the ratio of the two passband frequencies has a wide tuning range with satisfactory return loss in the passband as well as good rejection levels in the stopband. The spurious peak near twice the center frequencies in microstrip realization is eliminated by adding compensation interdigital capacitors to the coupled-line sections. The circuit performance is validated by comparing the measured responses with the simulation data.

ACKNOWLEDGMENT

This work was supported in part by the National Science Council, Taiwan, under Grant NSC 98-2211-E-009-032-MY2 and Grant NSC 100-2221-E-182-059-MY2 and by the Chang Gung University, Taiwan, under Grant UERPD2A0021.

REFERENCES

1. Kuo, J.-T. and H.-S. Cheng, "Design of quasi-elliptic function filters with a dual-passband response," *IEEE Microwave Wireless Compon. Lett.*, Vol. 14, No. 10, 472–474, Oct. 2004.
2. Kuo, J.-T., T.-H. Yeh, and C.-C. Yeh, "Design of microstrip bandpass filters with a dual-passband response," *IEEE Trans. Microwave Theory Tech.*, Vol. 53, No. 11, 1331–1337, Apr. 2005.
3. Kuo, J.-T. and H.-P. Lin, "Dual-band bandpass filter with improved performance in extended upper rejection band," *IEEE Trans. Microwave Theory Tech.*, Vol. 57, No. 4, 824–829, Apr. 2009.
4. Mondal, P. and M. K. Mondal, "Design of dual-band bandpass filters using stub-loaded open-loop resonators," *IEEE Trans. Microwave Theory Tech.*, Vol. 56, No. 1, 150–154, Jan. 2008.
5. Ma, D., Z. Y. Xiao, L. Xiang, X. Wu, C. Huang, and X. Kou, "Compact dual-band bandpass filter using folded SIR with two stubs for WLAN," *Progress In Electromagnetics Research*, Vol. 117, 357–364, 2011.
6. Chen, C.-Y. and C.-C. Lin, "The design and fabrication of a highly compact microstrip dual-band bandpass filter," *Progress In Electromagnetics Research*, Vol. 112, 299–307, 2011.
7. Chen, C.-H., C.-S. Shih, T.-S. Horng, and S.-M. Wu, "Very miniature dual-band and dual-mode bandpass filter designs on an integrated passive device chip," *Progress In Electromagnetics Research*, Vol. 119, 461–476, 2011.
8. Chiou, Y.-C., C.-Y. Wu, and J.-T. Kuo, "New miniaturized dual-mode dual-band ring resonator bandpass filter with microwave C-sections," *IEEE Microwave Wireless Compon. Lett.*, Vol. 20, No. 2, 67–69, Feb. 2010.
9. Lugo, C. and J. Papapolymerou, "Multilayer dual-band filter using a reflector cavity and dual-mode resonators," *IEEE Microwave Wireless Compon. Lett.*, Vol. 17, No. 9, 637–639, Sep. 2007.
10. Lin, T.-W., U-H. Lok, and J.-T. Kuo, "New dual-mode dual-band bandpass filter with quasi-elliptic function passbands and controllable bandwidths," *IEEE MTT-S Int. Dig.*, 576–579, Jun. 2010.
11. Yang, R.-Y., H. Kuan, C.-Y. Hung, and C.-S. Ye, "Design of dual-band bandpass filters using a dual feeding structure and embedded uniform impedance resonators," *Progress In Electromagnetics Research*, Vol. 105, 93–102, 2010.

12. Tsai, C.-M., H.-M. Lee, and C.-C. Tsai, "Planar filter design with fully controllable second passband," *IEEE Trans. Microwave Theory Tech.*, Vol. 53, No. 11, 3429–3439, Nov. 2005.
13. Lee, H.-M. and C.-M. Tsai, "Dual-band filter design with flexible passband and bandwidth selections," *IEEE Trans. Microwave Theory Tech.*, Vol. 55, No. 5, 1002–1009, May 2007.
14. Liu, A.-S., T.-Y. Huang, and R.-B. Wu, "A dual wideband filter design using frequency mapping and stepped-impedance resonators," *IEEE Trans. Microwave Theory Tech.*, Vol. 56, No. 12, 2921–2929, Dec. 2008.
15. Guan, X., Z. Ma, P. Cai, Y. Kobayashi, T. Anada, and G. Hagiwara, "Synthesis of dual-band bandpass filters using successive frequency transformations and circuit conversions," *IEEE Microwave Wireless Compon. Lett.*, Vol. 16, No. 3, 110–112, Mar. 2006.
16. Lai, S.-W., "New dual-band bandpass filter with desired rejection response," M.S. Thesis, National Chiao Tung University, Hsinchu, Taiwan, Jun. 2010.
17. Chin, K.-S. and J.-T. Kuo, "Insertion loss function synthesis of maximally flat parallel-coupled line bandpass filters," *IEEE Trans. Microwave Theory Tech.*, Vol. 53, No. 10, 3161–3168, Oct. 2005.
18. Kuo, J.-T., S.-P. Chen, and M. Jiang, "Parallel-coupled microstrip filters with over-coupled end stages for suppression of spurious responses," *IEEE Microwave Wireless Compon. Lett.*, Vol. 13, No. 10, 440–442, Oct. 2003.
19. Press, W. H., S. A. Teukolsky, W. T. Vetterling, and B. P. Flannery, *Numerical Recipes in FORTRAN 77*, 2nd edition, Cambridge University Press, New York, 1992.
20. IE3D simulator, Zeland Software Inc., Jan. 2002.
21. Dydyk, M., "Accurate design of microstrip directional couplers with capacitive compensation," *IEEE MTT-S Int. Dig.*, 581–584, 1990.
22. Alley, G. D., "Interdigital capacitors and their application to lumped-element microwave integrated circuits," *IEEE Trans. Microwave Theory Tech.*, Vol. 18, No. 12, 1028–1033, Dec. 1970.